Effect of backing fibers on the thermoelastic stress analysis of multi-directional glass/epoxy laminates during fatigue loading

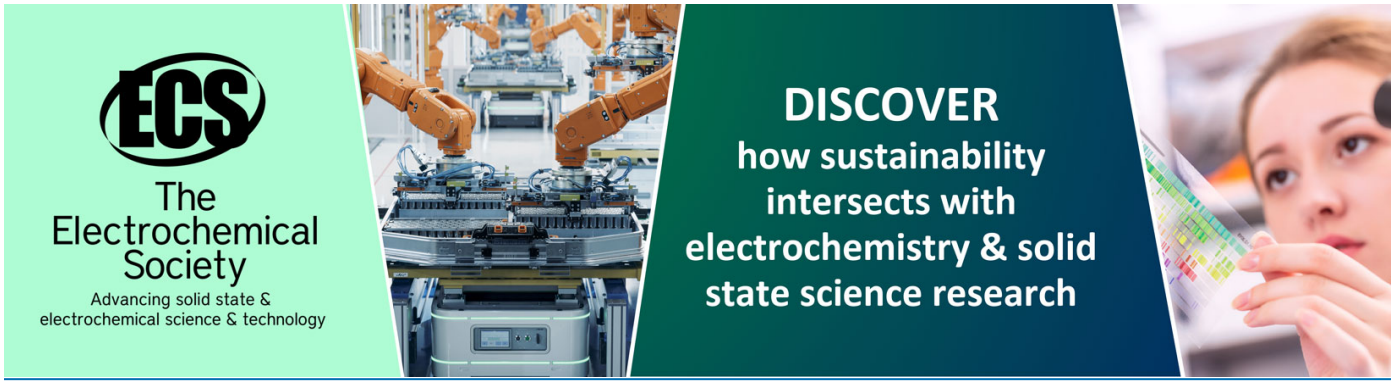

IOP Conf. Series: Materials Science and Engineering **942** (2020) 012040 doi:10.1088/1757-899X/942/1/012040

Effect of backing fibers on the thermoelastic stress analysis of multi-directional glass/epoxy laminates during fatigue loading

A Quinlan[1] , JM Dulieu-Barton[2] and O Castro[3]

[1]Department of Civil Engineering, Technical University of Denmark, Brovej 118, 2800 Kgs Lyngby, Denmark
[2] Department of Mechanical Engineering, University of Bristol, Queen's Building, University Walk, Bristol BS8 1TR, United Kingdom
[3] Department of Wind Energy, Technical University of Denmark, Frederiksborgvej 399, 4000 Roskilde, Denmark

E-mail: [1]alequ@byg.dtu.dk [2]janice.barton@bristol.ac.uk [3]osar@dtu.dk

Abstract. A preliminary study was conducted regarding Thermoelastic Stress Analysis (TSA) for use in monitoring stiffness degradation of multi-directional GFRP laminated specimens during tension-tension fatigue loading. The specimens were made from a non-crimp fabric consisting of UD fibers stitched to a layer off-axis backing fiber bundles. The thermoelastic responses of the UD surface and backing fiber surface were compared. It was observed that the thermoelastic response differed between two faces of the fabric and was influenced by the presence of backing fibers on the surface.

1. Introduction

Laminated fiber-reinforced polymer composites (FRPs) have become an attractive choice for weight critical engineering applications because their layup can be optimized for the design loads. But this positive attribute also makes FRPs difficult to characterize, especially for fatigue behavior. Fatigue in FRPs [1] occurs in fundamentally different mechanisms than metals, and FRP S-N curves are limited in application to the specific laminate studied. The current FRP design process involves extensive coupon testing to characterize a laminate's fatigue performance before prototype structures are created [2]. The time and cost of this process might be reduced by better understanding the micro-mechanics of FRP damage and fatigue and by performing more tests on FRP components and structures.

1.1. Damage in FRPs

One of the first damage mechanisms to occur in a laminate is matrix cracking [3]. While it is not a catastrophic damage mode, matrix cracking can lead to delamination [4], fiber breakage, and property degradation that all negatively affect a FRP structure's performance. Modeling and predicting the initiation, growth [5], and effects [6, 7] of matrix cracking is an active field of research. Some models [8] use micro-mechanics to predict the degradation of thermo-mechanical properties of a laminate containing matrix cracks. Experimental study is a critical part of developing, calibrating, and verifying these fatigue models. While this typically

occurs on material coupons, a multi-scale approach [2,9] is needed to evaluate the applicability of these models on components and sub-structures. Measuring the behavior of sub-components is more challenging than measuring coupon behavior, as the increase in both scale and complexity require additional consideration. In the case of evaluating applied stresses, the typical coupon method of calculating the nominal stress from the load-cell output and specimen cross sectional area cannot be applied, so an alternative method of "measuring" stress is thermoelastic stress analysis.

1.2. Thermoelastic Stress Analysis

Thermoelastic Stress Analysis (TSA) is a full-field non-contact measurement technique that assesses the stress amplitude on a material surface by obtaining a temperature change during cyclic loading using infrared imaging [10, 11]. The thermoelastic effect [12] states that the relationship between stress and temperature for an orthotropic material experiencing cyclic loading under adiabatic conditions is:

$$\Delta T = \frac{T_0}{\rho C_p}(\alpha_1 \Delta\sigma_1 + \alpha_2 \Delta\sigma_2) \tag{1}$$

where ρ is the density, C_p is the specific heat under constant pressure, T_0 is the temporal mean of the temperature signal, α_1 and α_2 are the linear coefficients of thermal expansion, σ_1 and σ_2 are the stresses, and the material's principal directions are notated as subscript 1 and 2. Rather than individually obtaining the exact values ρ, C_p, α_1 and α_2, it is often preferable to combine these into a quantity known as the thermoelastic constant, K, where

$$K_i = \frac{\alpha_i}{\rho C_p} \tag{2}$$

and substitute the K values into equation (1) to yield the following equation:

$$\Delta T = T_0(K_1\sigma_1 + K_2\sigma_2) \tag{3}$$

Procedures for calibrating K are documented in the literature [13, 14]. The calibration is carried out experimentally because the thermal properties of FRP laminates can vary between layups and production batches.

The application of TSA has increased in recent decades as thermal cameras have improved and reduced in cost. Studies have expanded from coupons to composite sub-components and structures [2, 11, 14–18]. To perform TSA, an infrared camera captures a series of image frames at a high rate so that the temperature waveform can be correlated with the load signal and extracted using a sine-fitting or lock-in algorithm. The temperature range and mean are then used in equation (3) to determine the stress values. Temperature is a scalar quantity, therefore it is necessary to *calibrate* ΔT to account for the orthotropic nature of the material by using some additional information from other experimental techniques.

The literature sources present varying interpretations of *which* stresses are analyzed during TSA. Three types of stresses considered are 1) surface resin stresses, 2) surface ply stresses, and 3) substrate ply stresses. Pitaressi et al [19] found that the surface resin rich layer (SRRL) acts as a strain witness and that the thermoelastic response is independent of the surface ply stresses. Bakis and Reifsnider [20] and Sambasivam et al [21] found that laminates with different surface ply orientations loaded to the same global strains do indeed have different thermoelastic responses. Crump and Dulieu-Barton [14] found that the thermoelastic response of a carbon fiber structure is influenced by the substrate plies during low frequency loading. These findings are not contradictory, but illustrate that the methodology for TSA will differ according to the material, surface coating, stress amplitude, and loading frequency.

1.3. Backing fiber bundles in wind turbine blade materials

The material under investigation in this paper is a glass fiber non-crimp fabric. Non-crimp fabrics have been used in the wind energy sector since the 1980's [22]. While some FRP components are made from pre-preg materials cured in an autoclave, composite structures that exceed the size of autoclaves, like wind turbine blades, are made by infusing resin into multi-directional (MD) or uni-directional (UD) fiber fabrics. Backing fibers are often used in UD fabrics to support the UD tows during processing [23] and are usually a small percent of the fiber weight, offering a minor contribution to the fabric's mechanical strength in the UD fiber direction. While useful for manufacturing, the backing fibers have been found as initiation sites for damage [23–27].

The objective of this work is to explore the effect of the backing fibers when using TSA to obtain a stress metric in a multi-directional laminate made with non-crimp fabric and to observe possible changes during fatigue loading. The work described in the paper provides initial steps in developing a TSA methodology for use on components and sub-structures made from a similar material under similar fatigue loadings.

2. Methodology

2.1. Specimens

Two types of specimens were made from E-glass and epoxy using UD non-crimp fabric with backing fibers running at 90°, 45°, and -45°angles relative to the UD tows. The backing fiber bundles cover only one surface, referred to here as the *backing fiber surface* (BFS), which is shown in figure 1.a. The opposite side contains only UD fibers and polyester threading, which is referred to here as the *uni-directional surface* (UDS) and is shown in figure 1.b. While all the fibers in the laminate are E-glass, the backing fibers are of a smaller diameter than the UD fibers. The fiber components of the non-crimp fabric are detailed in Table 1. While the total backing fiber weight is only 10% of the total, figure 1.a shows that about 60% of the fabric surface is covered by backing fiber bundles.

For specimen production, the non-crimp fabric was arranged according to the layups listed in Table 2, where the b indicates the location of the backing fibers surface. Vacuum assisted resin transfer molding (VARTM) was used to infuse the fabric with epoxy, which was then cured for 19 hours at 40°C, followed by 5 hours at 80°C. Rectangular specimens measuring 25 x 250 mm were made according to the ASTM guidelines [28]. The 8-ply laminates were 3.8 mm thick and had an approximate fiber volume fraction of 51%. The two specimens are referred to by their outer surfaces: the BFS specimen and the UDS specimen. The specimens were painted matte black to increase the emissivity of the surface.

2.2. Experimental procedure

The tests were performed using a 100 kN hydraulic axial test machine. The specimen temperature was monitored using an infrared camera with the specifications detailed in Table 3. An extensometer was used to measure the strain in the loading direction. Specimens were loaded to 8.25 ± 6.75 kN at a frequency of 5.1 Hz. The tests ran for 5000 cycles with sets of

Table 1. Fibers in Non-Crimp Fabric

Fiber Type	Fiber Diameter	% by Weight	% of Surface Area
UD	17 μm	90.5 %	40 %
90°	9 μm	5.5 %	60 %
± 45°	9 μm	4 %	

Table 2. Laminate layup configurations

Laminate	Layup
BFS	$[_b0°/_b60°/_b0°/_b\text{-}60°]_s$
UDS	$[0°_b/_b60°/_b0°/_b\text{-}60°]_s$

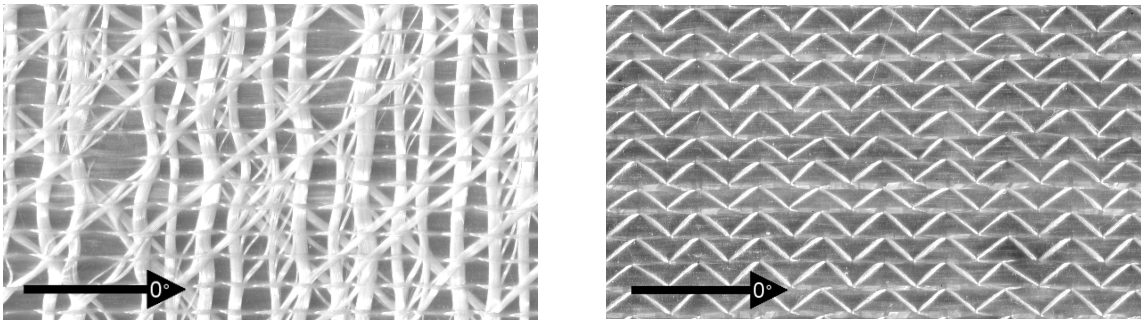

(a) (b)

Figure 1. Two surfaces of the UD non-crimp fabric with backing fibers: (a) BFS, (b) UDS

infrared images captured at intervals throughout the test.

Table 3. Thermal Camera Specifications

Make	Model	Resolution	Sample Rate	Sample Size
FLIR	SC6540	0.172 mm/pix	250 Hz	1500 frames

A motion compensation program was applied to the captured infrared image series. The motion compensated images were analyzed pixel by pixel using a least-squares algorithm developed at the University of Southampton. A sinusoid was fit to the data to compute the temperature's mean, amplitude, and phase as follows:

$$T(x,y,t) = T_0(x,y) + 0.5\Delta T(x,y)\cos(2\pi f_0 t + \phi(x,y)) \tag{4}$$

where x and y are the pixel coordinates, t is time, f_0 is the loading frequency, and ϕ is the phase angle.

3. Results and Discussion

The plots in figure 2 show the thermo-mechanical responses of the specimens as they undergo fatigue loading. Both the BFS specimen and the UDS specimen show similarly shaped stiffness degradation curves in figure 2.a, though the UDS specimen has a slightly higher initial modulus in the longitudinal direction. Consequentially, the UDS specimen experiences a slightly lower longitudinal strain in figure 2.b. The bulk heating of the laminates during the fatigue tests are similar in figure 2.c, with the temperature difference between the specimens remaining below 1°C throughout the test. Large changes in temperature affect the specific heat of GFRP, which is estimated to increase by about 3% over the duration of this test according to the equations provided in [29]. However, the temperature difference between the two specimens at a given cycle count is small enough that the specific heat can be assumed to be the same and the $\frac{\Delta T}{T_0}$ terms can be directly compared.

3.1. Thermoelastic response evolution

Although the nominal stress remains the same throughout the loading, the stress on the 0°plies is expected to increase as the ±60°plies degrade. Using the rough assumption that matrix damage occurs only in the ±60°plies and that no fiber breakage occurs in the 0°laminate, classical laminate theory [30], CLT, suggests that the observed 7% drop in global stiffness would

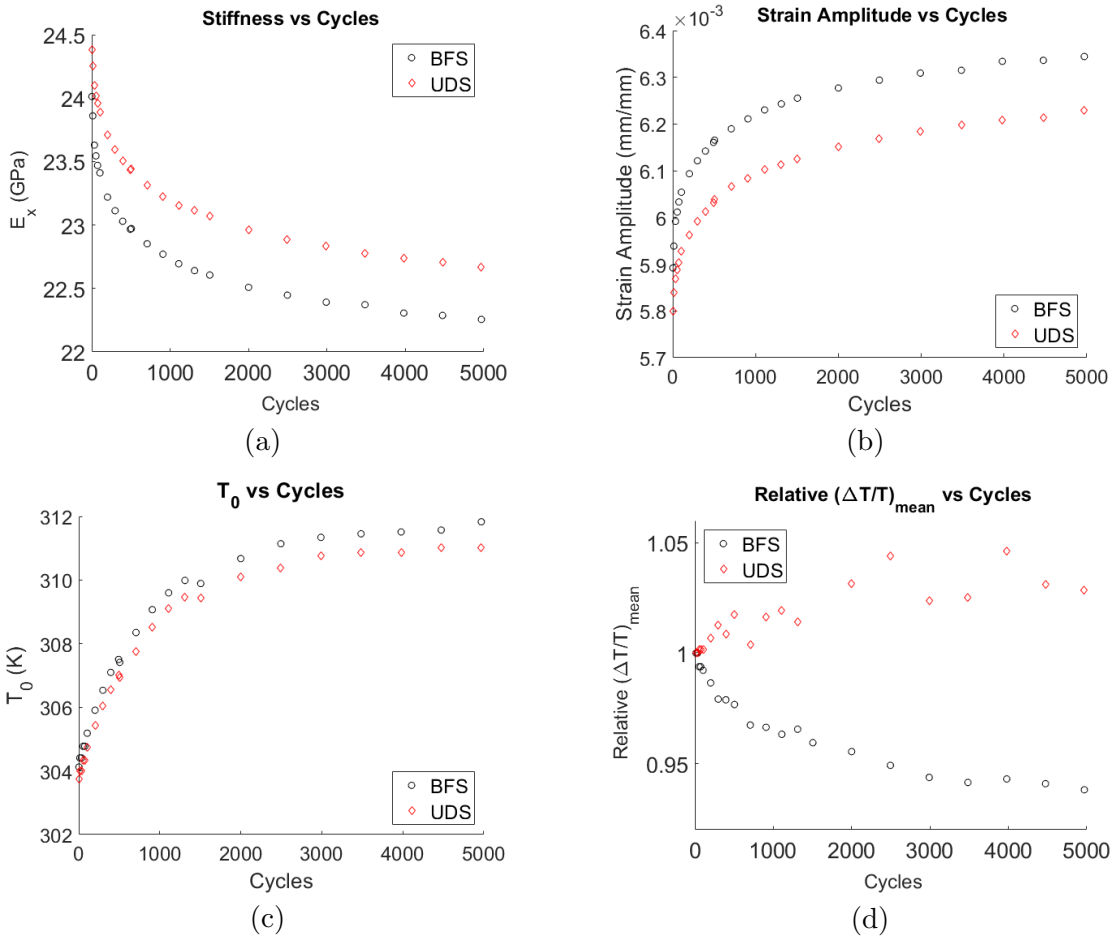

Figure 2. Evolution of the thermo-mechanical responses of the Backing Fiber Surface laminates and UD Surface laminates

correspond with an increase in the UD ply stresses by 7% in the longitudinal direction, while the transverse stresses remain close to 0. According to equation (3), these stress increases would result in a 7% increase in the thermoelastic response of the surface, assuming that the K values are unchanged.

Figure 2.d shows the mean $\frac{\Delta T}{T_0}$ term taken over the central region of the specimen. The average thermoelastic response of the UDS specimen increases by about 2% over the 5000 cycles, but the BFS specimen exhibits a decrease in thermoelastic response. This discrepancy suggests that the CLT approach might not fully account for the thermoelastic response.

Considering the surface resin rich layer (SRRL) approach [19], the SRRL should have a stress that increases proportionally with the laminate strains, assuming that laminate strains are fully transferred into the SRRL. Because the longitudinal strain increased by about 7% over the duration of the test, the thermoelastic response is also expected increase.

3.2. Surface texture thermoelastic response

The thermoelastic responses ($\frac{\Delta T}{T}$) from both specimens are shown in figure 3. As shown in figures 3.b and 3.d, the UDS specimen does not have clearly recognizable regions, but shows variation in thermoelastic response that is suspected to be caused by the surface roughness. In contrast, figures 3.a and 3.c show clear patterns on the BFS specimen that match with the regions of the surface. The most clear features are the horizontal lines corresponding to the

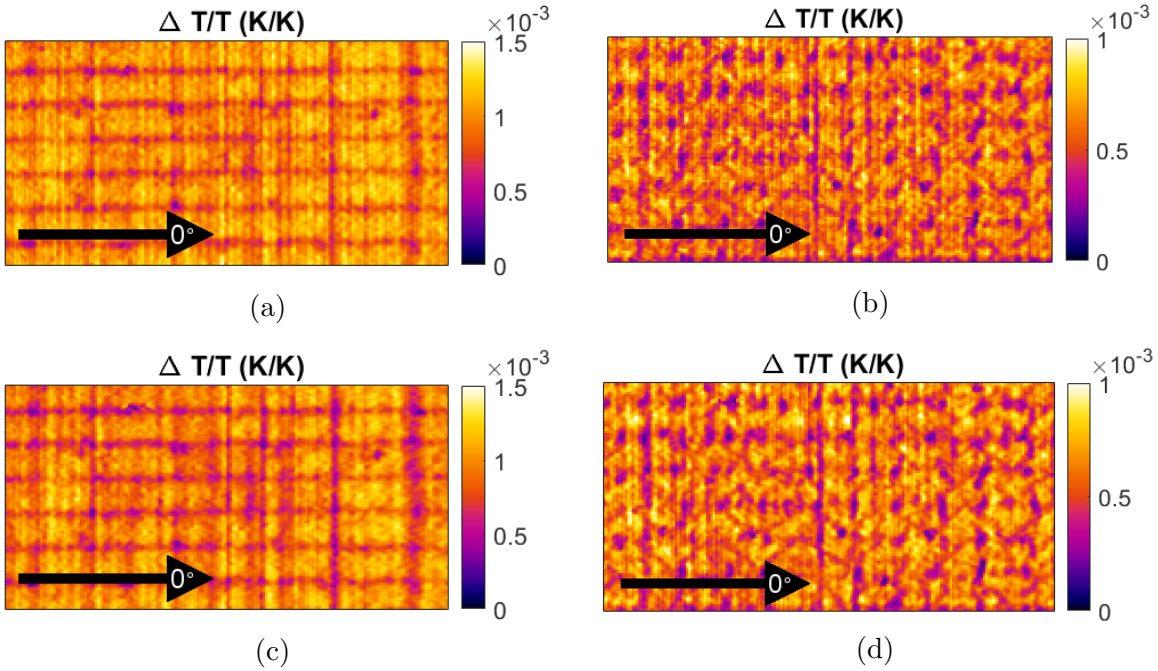

Figure 3. Thermoelastic responses of the specimen surfaces: (a) Test start - BFS, (b) Test start - UDS, (c) Test end - BFS, and (d) Test end - UDS. The horizontal lines are resin rich regions and the vertical lines are backing fibers.

matrix rich regions between the tows. The vertical lines correspond to the 90°backing fibers and become darker as the number of cycles increase. The thermoelastic response field from the BFS specimen shows agreement with Sambasivam [21] in that the texture of the surface ply is detectable through the surface resin layer. This, in addition to the mean thermoelastic response decreasing as the global strain increases, suggests that SRRL cannot account for the entirety of the thermoelastic response in these specimens. The possible lack of conformity to either the SRRL or CLT predictions could be attributed to many factors. First, the material properties of the laminate can change during the test: the specific heat of GFRP could be changing around 3% and the CTE can change during matrix cracking. Also, the surface resin layer may have uneven thickness across the fabric texture. The influence of the sub-surface layers and other non-adiabatic effects could also influence the thermoelastic response.

To further investigate the BFS's mean $\frac{\Delta T}{T}$ evolution in figure 2.d, the response of smaller regions are shown in figure 4. The backing fiber region shows a large decrease in $\frac{\Delta T}{T}$ over the first 500 cycles and then a downward trend afterwards, while the UD region stays relatively flat initially before exhibiting a slight downward trend. As the backing fibers were covering about 60% the surface, it appears that it was their stress changes that were responsible for the decrease in the mean thermoelastic response. Initially, the stiffness in the loading direction of the backing fibers was an order of magnitude lower than the UD tows, so a large stress difference between the features was expected. By the end of the test, cracks were observed in the backing fiber bundles, but not in the UD fiber tows. This may have caused an increase in the stress difference between the backing fibers and UD tows, resulting in a larger contrast in thermoelastic response between the regions.

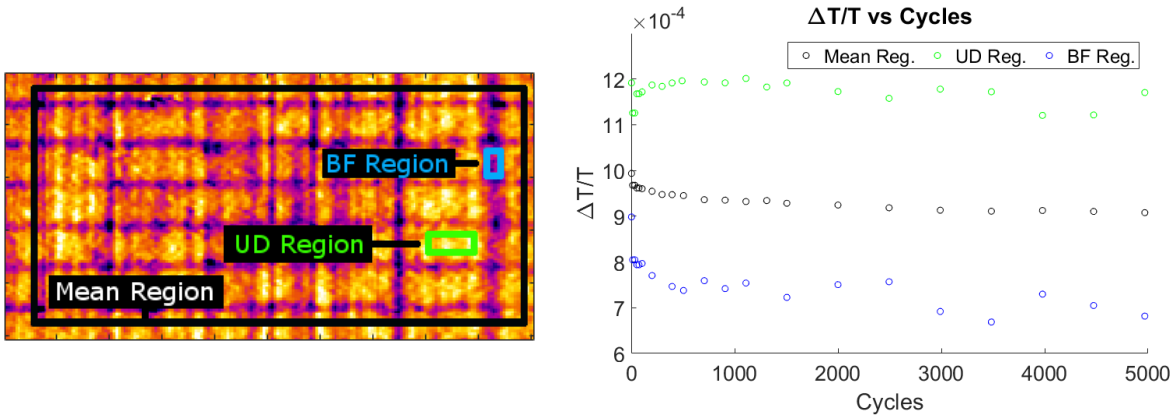

Figure 4. Evolution of thermoelastic response in different regions of the BFS specimen. The black, green, and blue sub-regions on the left correspond with the plot colors on the right.

3.3. Effect of cracks in BFS specimens

After 5000 cycles, many more matrix cracks were observed in the 90°backing than the 0°UD fibers. A transilluminated white light image is presented in figure 5 where the surface cracks are clear at 90°and ±45°, along with the 60°cracks of the sub-surface ply, while there are little to no cracks in the 0°tows on the surface ply. Matrix cracking occurs under transverse [8] and shear loads because of mode I and mode II crack opening [5], so the global longitudinal load acted normal to the 90°backing fiber bundles and facilitated matrix crack growth. In contrast, the longitudinal stress that dominated in the UD tows did not cause crack growth. Any cracking in the UD tows under this longitudinal load would have been caused by the transverse stress developed by the mismatch in Poisson's ratio between the surface ply and the laminate. When matrix cracking occurs, the effective thermoelastic properties decay [8], including the stiffness and the coefficient of thermal expansion α, which are specifically important to TSA. Because the different orientations of fibers had different crack densities, the stresses and thermoelastic response of the BFS specimen surface diverged across the features.

4. Conclusion

Two mechanically similar specimens were tested, with one having it's backing fibers layer exposed and the other having the surface layer flipped so that the UD fibers were exposed. The two specimens exhibited similar stiffness degradation behaviors, but had different thermoelastic responses. The response of neither laminate matched the expectations from the simplified Classical Laminate Theory or Surface Resin Rich Layer methods, which suggests that further work is needed to account for additional effects. The presence of backing fibers on the BFS specimen influenced its thermoelastic response evolution in a non-homogeneous manner as the damage level increased. This was caused by the different levels of stress induced in the UD and backing fibers of different angles. This non-homogeneous nature changed during fatigue loading, likely due to ma-

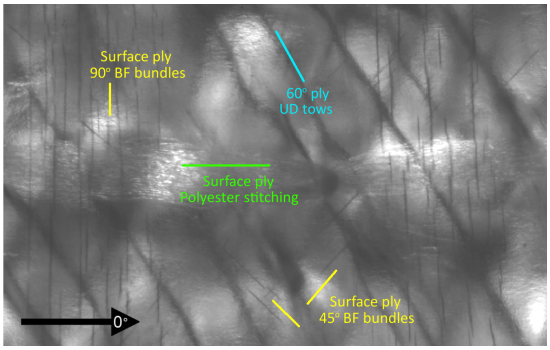

Figure 5. Photograph of a back-lit specimen after 5000 cycles, with surface cracks in 90°and ±45°backing fibers, and sub-surface cracks in ±60°plies.

trix crack development in the backing fiber bundles. Therefore, the UDS configuration appears to be preferable for use in future structural tests, as it avoids the potential influence of backing fibers on the TSA results.

The results presented in this paper encourage future work to both better understand the effects of backing fibers on TSA and how fatigue damage affects the material properties that influence the thermoelastic response. Examples of future work include:

- Testing specimens without paint on the surface so that the matrix crack density evolution can be recorded and compared with the TSA results
- Measuring full-field strains with Digital Image Correlation
- Testing uni-directional specimens with the layups $[_b0/_b0]_s$ and $[0_b/_b0]_s$ so the influence of the $\pm 60°$plies will be removed
- Testing specimens at different loading amplitudes and frequencies to observe possible non-adiabatic effects

Acknowledgments
This study was conducted as part of the CASMaT Initiation Project undertaken as part of Villum Center for Advanced Structural and Material Testing (grant no. VKR 023193).

References

[1] Van Paepegem W and Degrieck J 2002 *Int J Fatigue* **24** 747–62
[2] Bull D, Barton J, Thomsen O, Butler R, Rhead A, Fletcher A and Potter K 2017 *ICCM21*
[3] Quaresimin M 2018 *Comprehensive Composite Materials II* ed Beaumont P W and Zweben C H (Oxford: Elsevier) pp 249–74 ISBN 978-0-08-100534-7
[4] Carraro P A, Novello E, Quaresimin M and Zappalorto M 2017 *Compos. Struct.* **176** 420–32
[5] Carraro P, Maragoni L and Quaresimin M 2017 *COMPOS SCI TECHNOL* **145** 24–39
[6] Quaresimin M, Susmel L and Talreja R 2010 *Int J Fatigue* **32** 2–16
[7] Castro O and Branner K 2019 *ICCM22*
[8] Varna J 2016 *Modeling Damage, Fatigue and Failure of Composite Materials* Woodhead Publishing Series in Composites Science and Engineering ed Talreja R and Varna J (Woodhead Publishing) pp 243 – 87 ISBN 978-1-78242-286-0
[9] Talreja R 2006 *J. Mater. Sci.* **41** 6800–12
[10] Dulieu-Barton J M 2012 *Optical Methods for Solid Mechanics: A Full Field Approach* pp 345–66
[11] Dulieu-Barton J and Crump D 2011 *Experimental and Applied Mechanics* vol 6 (Springer) pp 259–66
[12] Stanley P 2008 *Strain* **44** 285–97
[13] Emery T, Dulieu-Barton J, Earl J and Cunningham P 2008 *COMPOS SCI TECHNOL* **68** 743–52
[14] Crump D and Dulieu-Barton J 2012 *Experimental mechanics* **52** 829–42
[15] Fortunato I J, Bull D J, Dulieu-Barton J M, Thomsen O T *et al.* 2019 *ICCM22*
[16] Salerno A and Costa A 2010 *ICEM 2010* vol 6
[17] Paynter R and Dutton A 2003 *Strain* **39** 73–8
[18] Waugh R C, Dulieu-Barton J M and Quinn S 2015 *ICEM 2014*
[19] Pitarresi G, Conti A and Galietti U 2005 *Applied Mechanics and Materials* vol 3 pp 167–72
[20] Bakis C E and Reifsnider K L 1991 *J COMPOS MATER* **25** 809–30
[21] Sambasivam S, Quinn S and Dulieu-Barton J 2009 *ICCM17*
[22] Adolphs G and Skinner C 2011 *Non-Crimp Fabric Composites* (Elsevier) pp 481–95
[23] Zangenberg J, Brøndsted P and Gillespie Jr J W 2014 *J COMPOS MATER* **48** 2711–27
[24] Jespersen K M, Glud J A, Zangenberg J, Hosoi A, Kawada H and Mikkelsen L P 2018 *Compos. Part A Appl. Sci. Manuf.* **109** 481–97
[25] Jespersen K M and Mikkelsen L P 2017 *COMPOS SCI TECHNOL* **153** 261–72
[26] Jespersen K M, Zangenberg J, Lowe T, Withers P J and Mikkelsen L P 2016 *COMPOS SCI TECHNOL* **136** 94–103
[27] Mikkelsen L P 2020 *Fatigue Life Prediction of Composites and Composite Structures* (Elsevier) pp 569–603
[28] ASTM 2017 *ASTM International*
[29] Kalogiannakis G, Van Hemelrijck D and Van Assche G 2004 *J COMPOS MATER* **38** 163–75
[30] Daniel I M, Ishai O, Daniel I M and Daniel I 1994 *Engineering mechanics of composite materials* 2nd ed (Oxford university press New York)